PERGAMON

International Journal of Rock Mechanics & Mining Sciences 37 (2000) 1103–1113

International Journal of
Rock Mechanics
and Mining Sciences

www.elsevier.com/locate/ijrmms

The double torsion loading configuration for fracture propagation: an improved methodology for the load-relaxation at constant displacement

M. Ciccotti*, G. Gonzato, F. Mulargia

Dipartimento di Fisica, Settore di Geofisica, Università di Bologna, Viale Berti Pichat 8, 40127, Bologna, Italy

Accepted 27 June 2000

Abstract

For most materials the dynamics of subcritical crack propagation during stress-corrosion can be described uniquely by a relationship between the mode-I stress intensity factor K_I and the crack velocity v that generally has the form of a power law. In last 30 years, the double-torsion load-relaxation test has shown to be the most reliable method for measuring such a relation. The standard analysis, developed by Evans (J Mater Sci 1972;7:1137–46), is based on an analytical approxatimation that fails to accurately describe the specimen compliance outside a narrow region in the center of the specimen. This paper deals with the implications on data inversion of the exhaustive three-dimensional finite-element analysis recently performed by Ciccotti (J Am Ceram Soc 2000, in press) on double-torsion specimens. The results are presented in terms of corrective coefficients to the classical analytical approximation. A full methodology is developed for the numerical implementation of such corrections. By numerically simulating some relaxation tests, the classical analysis based on the analytical approximation is shown to generally underestimate the stress-corrosion index up to 30% even if the most conservative operational constraints are satisfied. On the contrary, the operational constraints can be comfortably relaxed as a consequence of the capability of correcting the finite size effects in relation to the different experimental parameters.

1. Introduction

For most materials the dynamics of subcritical crack propagation during stress-corrosion can be described uniquely by a relationship between the mode-I stress intensity factor K_I and the crack velocity v that generally has the form of a power law [1]:

$$v = AK_I^n \tag{1}$$

with parameters A and n (the latter called the stress-corrosion index) depending on the materials properties and on environmental conditions.

In last 30 years, the double-torsion load-relaxation method has been widely used as the most reliable method for measuring subcrtitical crack growth curves ($v-K_I$) owing to the great stability of the four-point bending loading configuration and since it does not require the difficult monitoring of the crack length during the test.

A typical double-torsion (hereafter referred to as DT) specimen is shown in Fig. 1(a). According to Williams and Evans [4], K_I is evaluated by

$$K_I = \sqrt{EG} = Pw_m\sqrt{\frac{(1+v)}{\eta W d^3 d_n}}, \tag{2}$$

where E is the Young modulus, G the strain-energy release rate, P the applied load, w_m the moment arm of the torsion, v the Poisson's ratio, W the specimen width, d the specimen thickness, d_n the thickness of the specimen along the groove (see Fig. 1(b)), and η a corrective factor depending on the ratio W/d [5] (Evans [1] assumes $\eta = 1/3$ for thin specimens).

The crack velocity v is obtained using the load relaxation data together with a single measure of the initial or final crack length, provided that this is "far" from the ends of the specimen [4]:

$$v = -\phi a_{i,f} P_{i,f} \frac{1}{P^2}\frac{dP}{dt}, \tag{3}$$

*Corresponding author. Tel.: +390-51-20-95001; fax: +390-51-20-95058.

E-mail address: matteo@ibogfs.df.unibo.it (M. Ciccotti).

1365-1609/00/$ - see front matter
PII: S1365-1609(00)00045-9

where t is time, a the crack length (measured on the opening side of the specimen, starting from the loading points), and the subfixes i and f denote reference measurements taken at the beginning or at the end of the run. The factor $\phi = d_n/\sqrt{\Delta a^2 + d_n^2}$ was introduced by Evans [1] to take the inclination of the crack front into account (Fig. 1(c)). An improved calculation of ϕ can be found in [6].

This approach has been followed by several authors, but the measurements of the $v-K_I$ curves, even if measured in the same laboratory, are unavoidably marred by considerable scatter [7,8]. The reason for this variability is the heterogeneity of the rock samples combined with the sensitivity to environmental conditions and with the difficulty and cost of preparing specimens with low geometrical tolerances. In the present work, we will show that a substantial part of the scatter among different measurements is due to Evans' model not describing the effective deformation of a realistic DT specimen with sufficient accuracy.

The analytical approximation proposed by Evans was based on the following assumptions: the DT specimen is a symmetrical system of two independent plates, each of which subjected to simple torsion, with length equal to the crack length. The part of the specimen beyond the fracture tip is considered undeformed. The compression induced by torsion at the contact zone of the two plates on the upper face is ignored. Moreover, the presence of the side-groove, the effect of its shape, and the presence of the initial notch are ignored as well. Finally, the effect of the inclination of the crack front is only taken into account for what concerns the crack velocity, but not for G.

Some aspects of the problem have already been discussed in the literature [9–12]. Experiments carried out by Shetty and Virkar [13] showed that Eq. (2) overestimates K_I for short crack lengths, and underestimates it for long crack lengths. The same authors proposed the definition of an operational range for crack length, as the range in which the deviations of K_I from the value calculated through Eq. (2) were within 5%. Another inference on the acceptable operational range was obtained through a finite-element analysis of a DT specimen with an inclined crack front by Trantina [14], who nevertheless left unexplored the influence of the side groove, of its geometry and of the initial notch.

Ciccotti [2] investigated the importance of all these factors in an exhaustive three-dimensional finite-element analysis of the problem, and calculated the corrective coefficients to be applied to Evans' equation for G, as a function of the combination of each parameter with crack length and specimen dimensions. The finite-element mesh was made of about 500 quadratic brick elements, and represented a realistic specimen with side-groove, initial notch, and curved crack-front (see Fig. 2).

The aim of the present study is to define a new methodology for the analysis of the double-torsion load-relaxation constant-displacement tests, based on the use of the corrective coefficients obtained by the finite-element analysis. For a given specimen geometry, the corrective coefficients are dependent on the crack length, and therefore they are not constant during the relaxation test. As a consequence, the estimation of K_I must be corrected during the test and, since the inversion of the crack velocity v is affected in a non-linear way, the $v-K_I$

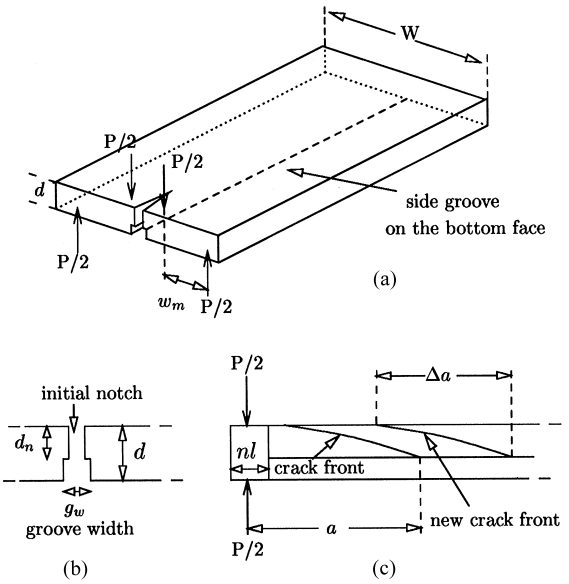

Fig. 1. The sketch of a double-torsion specimen: (a) general view, (b) axial cross-section, (c) longitudinal cross-section (modified after Atkinson [3]).

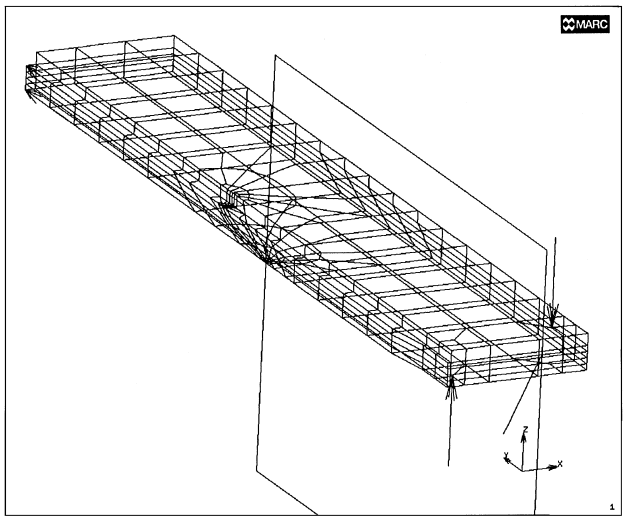

Fig. 2. The finite-element mesh. The model represents one half of a DT specimen. The remaining part is replaced by symmetry conditions and by a contact surface in the ruptured interface. The side-groove and initial notch are reproduced. The crack front is curved as observed in the experiments.

curve and the stress-corrosion index result to be significantly altered.

2. Corrective factors ξ and ψ

Evans' model leads to a linear dependence of the compliance on the crack length a:

$$C = \frac{y}{P} = \frac{w_m^2 a}{\eta W d^3 \mu} = Ba, \tag{4}$$

where y is the constant displacement imposed at the loading points. Experimental compliance-calibrations [1] lead to a more general affine relation $C = Ba + D$. Since G is related to the first derivative of the compliance,

$$G = -\left(\frac{\mathrm{d}U}{\mathrm{d}A}\right)_y = \frac{P^2}{2d_n}\frac{\mathrm{d}C}{\mathrm{d}a} \tag{5}$$

it appears to be independent of the crack length.

The finite-element analyses of Trantina [7] and Ciccotti [2] showed that the dependence of C on the crack length contains some weak nonlinear terms, hardly appreciable through experimental compliance-calibrations, which nevertheless produce significant variations in the first derivative, making G dependent on the crack length.

In order to account for such non-linear terms, a corrective factor ξ dependent on the crack length a has been introduced in Evans' equation for the compliance

$$C(a) = \frac{y}{P} = \xi(a)Ba = \xi(a)C^{\mathrm{E}}(a), \tag{6}$$

where the superscript E stands for "Evans' model" and B is the proportionality constant of Eq. (4). Taking the first derivative of Eq. (6), another corrective coefficient ψ is obtained that has to be applied to Evans' equation for the constant-displacement G,

$$G_y(a,P) = (\xi(a) + a\frac{\mathrm{d}\xi(a)}{\mathrm{d}a})G_y^{\mathrm{E}}(P) = \psi(a)G_y^{\mathrm{E}}(P). \tag{7}$$

The finite-element analysis produced the values of ξ and ψ calculated for five different crack lengths for each set of geometric parameters of the specimens. The values of the ξ coefficients are reported here in Tables 1–4. The values of ψ were already reported in [2], where the discussion was focused on the corrections to G.

The corrective coefficients for specimens with length $L = 17$ cm and width $W = 6$ cm were reported in Figs. 3 and 4 as an example. The shape of the function $\psi(a)$ is characterized by a positive trend with a flatter region in the center of the specimen, and strong deviations moving towards the ends. The scatter introduced by the dependence on the geometric parameters is considerable.

The overall behavior of the corrective functions can be understood as follows. Using the two independent torsion bars model, the compliance falls linearly to zero together with the length a of the bars. In real specimens with short cracks, the deformation also affects the region beyond the crack, so that the compliance is larger and its slope is lower. As a consequence, when the crack length approaches zero, ξ increases and diverges to infinity and ψ decreases towards zero. When the crack approaches the end of the specimen, the unfractured portion becomes very weak, so that the compliance increases faster than predicted by Evans' equation, and diverges when the crack reaches the end (i.e., when the specimen fails). As a consequence, both ξ and ψ diverge to infinity for $a \to L$.

3. New equations for K_I and v

We will now discuss how the introduction of crack-length dependent corrective factors affects the estimates of K_I and v. As far as K_I is concerned, the square root of the corrective coefficients ψ should be used (see Eq. (2)):

$$K_I(a,P) = \sqrt{\psi(a)}K_I^{\mathrm{E}}(P). \tag{8}$$

The calculation of the crack velocity is based on the derivation of the crack length $a(t)$, which is inverted from the load relaxation curve $P(t)$, through the constant displacement condition. Differentiation of Eq. (6) for constant displacement leads to

$$\left(\frac{\mathrm{d}a}{\mathrm{d}t}\right)_y = -\frac{\xi(a)}{\psi(a)}\frac{a}{P}\frac{\mathrm{d}P}{\mathrm{d}t}, \tag{9}$$

where $P(t)$ is the measured relaxation load, and $a(t)$ has to be inverted from $P(t)$ using the relation

$$y = C(a(t))P(t) = C(a_{\mathrm{i,f}})P_{\mathrm{i,f}}, \tag{10}$$

where y is the constant displacement, and the subfixes i or f again denote a reference measurement taken at the beginning or at the end of the test. Thus,

$$a(t) = C^{-1}\left(\frac{C(a_{\mathrm{i,f}})P_{\mathrm{i,f}}}{P(t)}\right). \tag{11}$$

Substituting Eq. (11) into Eq. (9) and multiplying by the appropriate factor ϕ we obtain

$$v = \phi\left(\frac{\mathrm{d}a}{\mathrm{d}t}\right)_y = -\phi\,\frac{\xi(a_{\mathrm{i,f}})}{\psi\left(C^{-1}\left(\frac{C(a_{\mathrm{i,f}})\cdot P_{\mathrm{i,f}}}{P}\right)\right)}\frac{a_{\mathrm{i,f}}P_{\mathrm{i,f}}}{P^2}\frac{\mathrm{d}P}{\mathrm{d}t}. \tag{12}$$

Eq. (11) also has to be substituted into Eq. (8) to calculate K_I as a function of time, and thus produce the subcritical crack-growth curve $v-K_I$.

The above corrections affect both K_I and v in a non-linear way which changes the overall shape of the logarithmic $v-K_I$ curve, both in its location and slope. The corrections reduce K_I in the first part of the test, when it is larger, and increase it when it is lower, thus resulting in a rise in the slope, i.e., the stress-corrosion index n, in agreement with [13]. Note that the correction

Table 1
The corrective factors ξ for specimens of length $L = 17$ cm and width $W = 6$ cm; d the specimen thickness, d_n is the thickness along the groove, g_w is the groove width in mm, nl is the notch length in cm, $c = \Delta a/d_n$ is the inclination of the crack front. Some data missing because the curved crack front would cross the initial notch

d_n/d	g_w	nl	c	$a = 4.5$cm	$a = 6.5$ cm	$a = 8.5$ cm	$a = 10.5$ cm	$a = 12.5$ cm
1	0	0	0	1.101	1.057	1.036	1.023	1.018
1	0	0	2	0.892	0.902	0.916	0.925	0.936
1	0	0	4	0.752	0.787	0.827	0.853	0.875
2/3	2	0	0	1.221	1.141	1.100	1.077	1.069
2/3	2	0	2	1.156	1.095	1.065	1.047	1.042
2/3	2	0	4	1.081	1.042	1.024	1.014	1.013
2/3	4	0	0	1.285	1.192	1.145	1.118	1.110
2/3	4	0	2	1.215	1.143	1.107	1.087	1.082
2/3	4	0	4	1.134	1.085	1.062	1.050	1.049
1/2	2	0	0	1.395	1.267	1.198	1.159	1.150
1/2	2	0	2	1.354	1.238	1.175	1.141	1.132
1/2	2	0	4	1.304	1.202	1.148	1.118	1.111
1/2	4	0	0	1.513	1.365	1.282	1.238	1.233
1/2	4	0	2	1.471	1.334	1.258	1.218	1.213
1/2	4	0	4	1.412	1.292	1.226	1.191	1.186
1	0	2	0	1.111	1.063	1.040	1.026	1.021
1	0	2	2	—	0.907	0.920	0.929	0.939
1	0	2	4	—	0.793	0.831	0.856	0.877
2/3	2	2	0	1.224	1.143	1.101	1.077	1.070
2/3	2	2	2	1.159	1.096	1.066	1.048	1.043
2/3	2	2	4	1.086	1.043	1.025	1.015	1.013
2/3	4	2	0	1.290	1.195	1.147	1.119	1.112
2/3	4	2	2	1.221	1.146	1.109	1.088	1.083
2/3	4	2	4	1.142	1.088	1.065	1.052	1.050
1/2	2	2	0	1.397	1.268	1.199	1.160	1.151
1/2	2	2	2	1.356	1.239	1.176	1.141	1.133
1/2	2	2	4	1.306	1.203	1.148	1.118	1.111
1/2	4	2	0	1.516	1.366	1.283	1.239	1.233
1/2	4	2	2	1.474	1.335	1.259	1.219	1.213
1/2	4	2	4	1.416	1.293	1.227	1.191	1.187

on the crack velocity v also affects the slope through the ψ coefficient in Eq. (12), which increases with a during the test. As a result, initial large velocities are increased and final low velocities are decreased, so that the slope n is further increased. The practical importance of the corrections to be applied to the stress-corrosion index n will be discussed in the following.

4. Numerical implementation

For each set of geometrical parameters, the finite-element analysis produced a set of five corrective coefficients ξ for the compliance and five coefficients ψ for its derivative, relative to different crack lengths.

The first operation is to determine a set of coefficients for the geometry of the specific specimen used in the test. In other words, the specimen geometry has to be interpolated from the set of tabulated geometries. Linear interpolation is generally adequate, except for the effect of specimen length which requires a scaling of the crack length.

The scaling of the crack lengths corresponding to the five corrective coefficients can only be effected for specimens with the same ratio $d : W : L$ explored here. Extrapolations far from such ratios would require further numerical analysis. Note that the scaling also affects the length of the notch and the position of the loading points, which has to be taken as a new reference for the measurement of the crack length.

Table 2
The corrective factors ξ for specimens of length $L = 17$ cm and width $W = 10$ cm

d_n/d	g_w	nl	c	$a = 4.5$ cm	$a = 6.5$ cm	$a = 8.5$ cm	$a = 10.5$ cm	$a = 12.5$ cm
1	0	0	0	1.085	1.037	1.020	1.016	1.034
1	0	0	2	0.764	0.783	0.819	0.850	0.891
1	0	0	4	0.615	0.659	0.719	0.767	0.815
2/3	2	0	0	1.223	1.135	1.098	1.086	1.108
2/3	2	0	2	1.103	1.048	1.029	1.029	1.054
2/3	2	0	4	1.010	0.979	0.975	0.983	1.012
2/3	4	0	0	1.289	1.186	1.142	1.128	1.154
2/3	4	0	2	1.166	1.096	1.071	1.068	1.098
2/3	4	0	4	1.067	1.023	1.013	1.020	1.052
1/2	2	0	0	1.456	1.305	1.235	1.210	1.238
1/2	2	0	2	1.381	1.251	1.192	1.173	1.202
1/2	2	0	4	1.313	1.201	1.153	1.140	1.169
1/2	4	0	0	1.595	1.414	1.330	1.303	1.343
1/2	4	0	2	1.518	1.358	1.285	1.265	1.305
1/2	4	0	4	1.442	1.301	1.240	1.225	1.265
1	0	2	0	1.101	1.042	1.022	1.018	1.035
1	0	2	2	—	0.788	0.822	0.853	0.892
1	0	2	4	—	0.665	0.723	0.769	0.817
2/3	2	2	0	1.232	1.137	1.099	1.087	1.108
2/3	2	2	2	1.113	1.051	1.030	1.029	1.055
2/3	2	2	4	1.021	0.982	0.976	0.983	1.012
2/3	4	2	0	1.301	1.189	1.143	1.129	1.154
2/3	4	2	2	1.178	1.100	1.072	1.069	1.099
2/3	4	2	4	1.082	1.027	1.015	1.021	1.053
1/2	2	2	0	1.461	1.306	1.235	1.210	1.239
1/2	2	2	2	1.387	1.252	1.192	1.174	1.203
1/2	2	2	4	1.320	1.203	1.153	1.140	1.170
1/2	4	2	0	1.602	1.415	1.330	1.303	1.344
1/2	4	2	2	1.526	1.359	1.286	1.265	1.305
1/2	4	2	4	1.451	1.304	1.241	1.226	1.265

Provided that the notch extends towards the center of the specimen past the loading points, the external part of the specimen does not affect the strain energy. As a consequence, the part of the notch that should be compared among different specimens is the one exceeding the position of the loading points. For example, if the notch is 2 cm long and the loading points are 0.5 cm from the end of the specimen, the effective length is 1.5 cm.

In Tables 1–4 some coefficients are missing. These correspond to the shortest crack length of notched specimens without groove, for which the meshes could not be drown since the large horizontal extension of the curved crack front would make it intrude in the initial notch. But these missing coefficients are necessary for the interpolation process, and their values were estimated by combining the coefficients relative to the corresponding unnotched specimens together with the weak effect of the presence of the notch observed on specimens with deeper grooves. The results are reported in Table 5.

The maximum crack front inclination in our numerical analysis was $c = \Delta a/d_n = 4$ due to the limitations in the skewness of the elements, necessary to perform an accurate numerical analysis. Even though the typical front inclination is $c = 5$ [1], the use of the finite-element analysis with $c = 4$ is recommended in order to guarantee reliable solutions.

Through interpolation among the lines of coefficients reported in the tables, we have now determined the set of five ψ and ξ values for the appropriate specimen geometry along with the five corresponding values of the crack length. Since the crack propagates during the experiment, both coefficients should be fitted with smooth functions of the crack length.

Table 3
The corrective factors ξ for specimens of length $L = 25\,\text{cm}$ and width $W = 6\,\text{cm}$

d_n/d	g_w	nl	c	$a = 5.5\,\text{cm}$	$a = 8.5\,\text{cm}$	$a = 12.5\,\text{cm}$	$a = 16.5\,\text{cm}$	20.5cm
1	0	0	0	1.075	1.036	1.014	1.003	0.998
1	0	0	2	0.894	0.915	0.932	0.940	0.948
1	0	0	4	0.763	0.827	0.871	0.894	0.911
2/3	2	0	0	1.173	1.100	1.057	1.036	1.029
2/3	2	0	2	1.119	1.064	1.033	1.017	1.013
2/3	2	0	4	1.056	1.024	1.005	0.996	0.995
2/3	4	0	0	1.230	1.144	1.094	1.069	1.063
2/3	4	0	2	1.172	1.106	1.069	1.050	1.045
2/3	4	0	4	1.104	1.062	1.039	1.027	1.025
1/2	2	0	0	1.321	1.196	1.123	1.087	1.079
1/2	2	0	2	1.287	1.174	1.108	1.075	1.069
1/2	2	0	4	1.244	1.146	1.089	1.061	1.055
1/2	4	0	0	1.429	1.278	1.189	1.145	1.142
1/2	4	0	2	1.393	1.254	1.173	1.133	1.130
1/2	4	0	4	1.343	1.222	1.151	1.116	1.113
1	0	2	0	1.081	1.040	1.016	1.005	1.000
1	0	2	2	—	0.919	0.934	0.942	0.950
1	0	2	4	—	0.831	0.873	0.896	0.912
2/3	2	2	0	1.175	1.101	1.058	1.036	1.030
2/3	2	2	2	1.121	1.065	1.034	1.018	1.013
2/3	2	2	4	1.059	1.025	1.006	0.997	0.995
2/3	4	2	0	1.233	1.146	1.096	1.070	1.064
2/3	4	2	2	1.175	1.109	1.070	1.051	1.046
2/3	4	2	4	1.108	1.064	1.040	1.028	1.026
1/2	2	2	0	1.322	1.197	1.124	1.087	1.080
1/2	2	2	2	1.288	1.174	1.109	1.075	1.069
1/2	2	2	4	1.245	1.147	1.090	1.061	1.056
1/2	4	2	0	1.431	1.279	1.190	1.146	1.142
1/2	4	2	2	1.395	1.255	1.174	1.134	1.131
1/2	4	2	4	1.345	1.223	1.152	1.117	1.114

An appropriate choice for smoothing the corrective factors $\psi(a)$ appears to be a least-squares third-degree polynomial fit. The corrective coefficients ξ are best approximated by fitting the normalized compliance $C(a)/B = \xi(a)a$ first. This can be done integrating the polynomial which fits ψ and choosing the constant to match the central coefficient. In this way, approximation inaccuracies below 1% on both coefficients can be obtained. Nevertheless, such a choice may sometimes produce appreciable errors on the values of ξ, especially at small or large crack lengths. If this is the case, a second-order polynomial fit for the normalized compliance will produce more accurate results. Any extrapolation out of the range explored by the present analysis is not recommended.

The interpolating function for the compliance has to be used together with the measurement of the initial or final reference point $a_{i,f}$, $P_{i,f}$, to invert the evolution of the crack length $a(t)$ from the relaxation data $P(t)$, using Eq. (10).

Finally, the corrected values of K_I and v during the relaxation test are calculated, and the complete $v-K_I$ curve is obtained. Then, the data related to region III should be isolated, and the stress-corrosion index n can be calculated by a least-squares linear fit.

5. Operational geometric constraints

The non-constancy of K_I along the specimen was already pointed out in the literature [13,14], a problem which was practically tackled by assuming an operational range for the crack length in which the classical Evans' analysis could be used. The operational range

Table 4
The corrective factors ξ for specimens of length $L = 25$ cm and width $W = 10$ cm

d_n/d	g_w	nl	c	$a = 5.5$ cm	$a = 8.5$ cm	$a = 12.5$ cm	$a = 16.5$ cm	20.5 cm
1	0	0	0	1.054	1.018	1.002	0.996	1.010
1	0	0	2	0.765	0.815	0.861	0.889	0.922
1	0	0	4	0.626	0.717	0.791	0.835	0.875
2/3	2	0	0	1.168	1.093	1.054	1.036	1.055
2/3	2	0	2	1.067	1.025	1.007	1.000	1.022
2/3	2	0	4	0.987	0.971	0.970	0.972	0.996
2/3	4	0	0	1.225	1.134	1.086	1.065	1.087
2/3	4	0	2	1.120	1.064	1.038	1.028	1.054
2/3	4	0	4	1.036	1.007	0.998	0.998	1.025
1/2	2	0	0	1.362	1.221	1.142	1.107	1.135
1/2	2	0	2	1.300	1.179	1.113	1.085	1.114
1/2	2	0	4	1.242	1.140	1.087	1.065	1.093
1/2	4	0	0	1.479	1.304	1.205	1.165	1.206
1/2	4	0	2	1.414	1.260	1.175	1.142	1.184
1/2	4	0	4	1.350	1.217	1.146	1.119	1.158
1	0	2	0	1.063	1.020	1.004	0.997	1.010
1	0	2	2	—	0.818	0.863	0.890	0.923
1	0	2	4	—	0.722	0.793	0.837	0.876
2/3	2	2	0	1.173	1.094	1.054	1.036	1.055
2/3	2	2	2	1.072	1.026	1.007	1.001	1.022
2/3	2	2	4	0.993	0.972	0.970	0.972	0.996
2/3	4	2	0	1.230	1.136	1.087	1.065	1.088
2/3	4	2	2	1.127	1.066	1.038	1.028	1.054
2/3	4	2	4	1.044	1.009	0.999	0.998	1.026
1/2	2	2	0	1.365	1.221	1.142	1.108	1.135
1/2	2	2	2	1.303	1.179	1.113	1.085	1.114
1/2	2	2	4	1.246	1.141	1.087	1.065	1.093
1/2	4	2	0	1.483	1.304	1.206	1.165	1.206
1/2	4	2	2	1.418	1.261	1.176	1.142	1.184
1/2	4	2	4	1.354	1.218	1.146	1.119	1.158

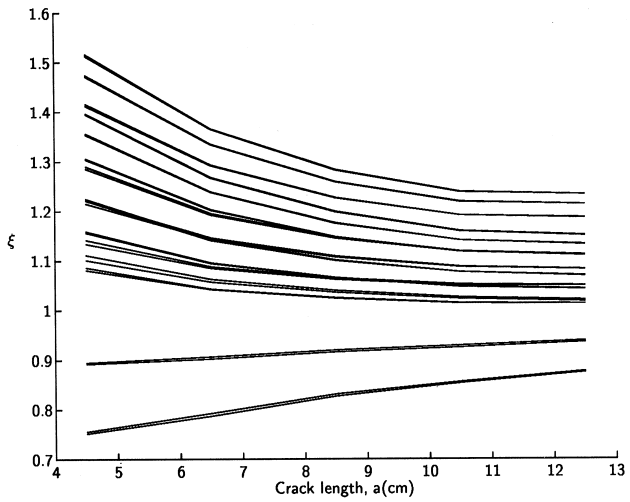

Fig. 3. The corrective coefficients of ξ for specimens with length $L = 17$ cm and width $W = 6$ cm. The different curves represent all combinations of the other geometric parameters.

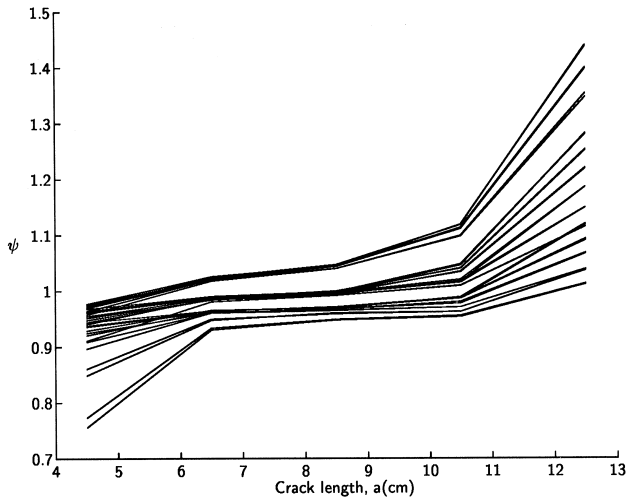

Fig. 4. The corrective coefficients of ψ for specimens with length $L = 17$ cm and width $W = 6$ cm. The different curves represent all combinations of the other geometric parameters.

Table 5
The corrective coefficients ξ and ψ reported here were estimated to fill the gaps in Tables 1–4 in the present paper and in Tables 1–4 in [2], where the corrective coefficients ψ are reported

L (cm)	17	17	17	17	25	25	25	25
W (cm)	6	6	10	10	6	6	10	10
c	2	4	2	4	2	4	2	4
ξ	0.895	0.756	0.772	0.624	0.896	0.765	0.769	0.631
ψ	0.849	0.756	0.657	0.520	0.920	0.890	0.825	0.755

Table 6
The crack length operational range defined as the region in which the variations of K_I with respect to the center of the specimen are within 5%. The symbols are the same as in Table 1. The specimen thickness is $d=7$ mm, and the crack front inclination is $c=4$ for all specimens

L	W	d_n/d	g_w	nl	$\frac{a_{min}}{W}$	$\frac{(L-a_{max})}{W}$
17	6	1	0	0	0.89	0.66
17	6	2/3	2	0	0.57	0.76
17	6	2/3	4	0	0.58	0.80
17	6	1/2	2	0	0.59	0.95
17	6	1/2	4	0	0.69	1.01
17	6	1	0	2	0.91	0.66
17	6	2/3	2	2	0.69	0.75
17	6	2/3	4	2	0.71	0.80
17	6	1/2	2	2	0.62	0.95
17	6	1/2	4	2	0.70	1.01
17	10	1	0	0	0.61	0.54
17	10	2/3	2	0	0.47	0.64
17	10	2/3	4	0	0.48	0.66
17	10	1/2	2	0	0.49	0.69
17	10	1/2	4	0	0.54	0.72
17	10	1	0	2	0.62	0.53
17	10	2/3	2	2	0.52	0.64
17	10	2/3	4	2	0.54	0.66
17	10	1/2	2	2	0.54	0.69
17	10	1/2	4	2	0.59	0.72
25	6	1	0	0	0.77	0.59
25	6	2/3	2	0	0.33	0.77
25	6	2/3	4	0	0.39	0.90
25	6	1/2	2	0	0.45	1.12
25	6	1/2	4	0	0.52	1.23
25	6	1	0	2	0.77	0.58
25	6	2/3	2	2	0.39	0.78
25	6	2/3	4	2	0.45	0.88
25	6	1/2	2	2	0.48	1.11
25	6	1/2	4	2	0.53	1.23
25	10	1	0	0	0.60	0.63
25	10	2/3	2	0	0.44	0.76
25	10	2/3	4	0	0.45	0.79
25	10	1/2	2	0	0.43	0.86
25	10	1/2	4	0	0.44	0.91
25	10	1	0	2	0.64	0.63
25	10	2/3	2	2	0.48	0.76
25	10	2/3	4	2	0.49	0.78
25	10	1/2	2	2	0.47	0.85
25	10	1/2	4	2	0.48	0.90

was defined as the one in which K_I remained constant within 5%.

According to the above constraint, the experimental study of Shetty and Virkar [13] determined as operational the following ranges of crack lengths:

$0.50W<a<L-1.00W$ for $d:W:L=1:31.25:75$,

$0.40W<a<L-0.80W$ for $d:W:L=1:50:75$.

The finite-element study of Trantina [14] determined the range:

$0.55W<a<L-0.65W$ for $d:W:L=1:10:20$.

The present numerical study allows a detailed and comprehensive analysis of the dependence of the operational range on the geometrical properties of the specimen (see Table 6). A general dependence on the $d:W:L$ ratio may be observed. At the same time, the depth and width of the groove are also important, while the presence of the initial notch has lesser effects. Only the ranges relative to the skewest crack fronts ($c=4$) have been reported because they are the only one close to the real shapes.

The range determined by Trantina was calculated for model specimens with a weak front inclination $c=1.7$ and should be compared with the ranges $0.50W<a<L-0.68W$ and $0.76W<a<L-0.70W$ obtained in the present study, respectively, for $c=0$ and 2 relative to specimens without notch and groove and with a $d:W:L$ ratio of $1:8.6:24.3$. The comparison can only be partial since the $d:W:L$ ratios are not coincident and the position of the loading points was presumably taken at the end of the specimen in Trantina's simulation. A detailed comparison with the ranges determined by Shetty and Virkar [13] is also impossible since their specimens are thinner than the ones considered here.

6. The "true" value of the stress-corrosion index

In order to investigate the effect of neglecting the use of the corrective coefficients, as it happened so far in all analyses, some relaxation experiments have been simulated numerically. A theoretical stress-corrosion $v-K_I$ curve was assumed with the form of a power law, as in Eq. (1), with the values of the parameters $n=40$ and $A=10^{-3}\,\mathrm{ms}^{-1}$ chosen as in typical igneous rocks [7].

Two specimens were simulated with geometries chosen in the explored set of parameters and the corresponding corrective curves were interpolated as described above. The first simulated specimen, 'Specimen 1', had geometrical parameters $L=17$ cm, $W=10$ cm, $d=7$ mm, $d_n/d=1/2$, groove width $g_w=2$ mm (see Fig. 1), notch length $nl=2$ cm, and crack front inclination $c=4$. The second simulated specimen, 'Specimen 2', had parameters $L=25$ cm,

$W = 10\,\text{cm}$, $d = 7\,\text{mm}$, $d_n/d = 1$, $g_w = 0\,\text{mm}$, $nl = 2\,\text{cm}$, and $c = 4$.

The third-order polynomials fitting the coefficients ψ for the two specimens were, respectively,

$$\psi(a) = 4.504 \times 10^{-4}a^3 - 1.690 \times 10^{-2}a^2 + 2.094 \times 10^{-1}a + 3.990 \times 10^{-2} \quad (13)$$

and

$$\psi(a) = 3.219 \times 10^{-3}a^3 - 6.977 \times 10^{-2}a^2 + 5.274 \times 10^{-1}a - 3.988 \times 10^{-1}. \quad (14)$$

The interpolating functions for the ξ coefficients were determined by interpolating the normalized compliance $C(a)/B = \xi(a)a$ with a second-order polynomial fit, and then dividing it by a. Respectively

$$\xi(a) = 5.991 \times 10^{-3}a + 8.100 \times 10^{-1} - 1.168\frac{1}{a}, \quad (15)$$

$$\xi(a) = 3.106 \times 10^{-2}a + 5.480 \times 10^{-1} + 2.881\frac{1}{a}. \quad (16)$$

The corrective functions of K_I for the two specimen geometries are plotted in Figs. 5 and 6. The operational ranges are indicated in these figures, together with the ranges explored by our finite-element study.

Several relaxations were simulated, using an initial load $P = 100$ kg and different values of the initial crack length (reported in Table 7).

The scheme of the simulation was as follows:

(a) use Eq. (8) to derive K_I from the initial load P, using the corrective coefficient ψ calculated on the initial crack length;
(b) use the theoretical relation Eq. (1) to obtain the crack velocity v;

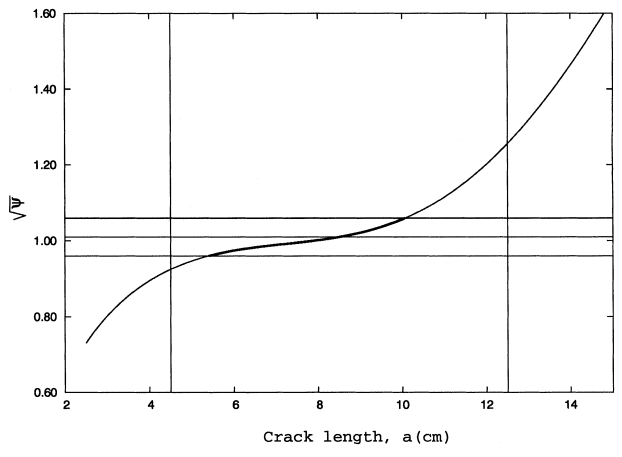

Fig. 5. The corrective function for K_I for the geometry called 'Specimen 1' ($L = 17\,\text{cm}$, $W = 10\,\text{cm}$, $d = 7\,\text{mm}$, $d_n/d = 1/2$, $g_w = 2\,\text{mm}$, $nl = 2\,\text{cm}$, $c = 4$). The vertical lines delimit the range explored in the present analysis. The horizontal lines define the operational range in which K_I is constant within 5% (thick line).

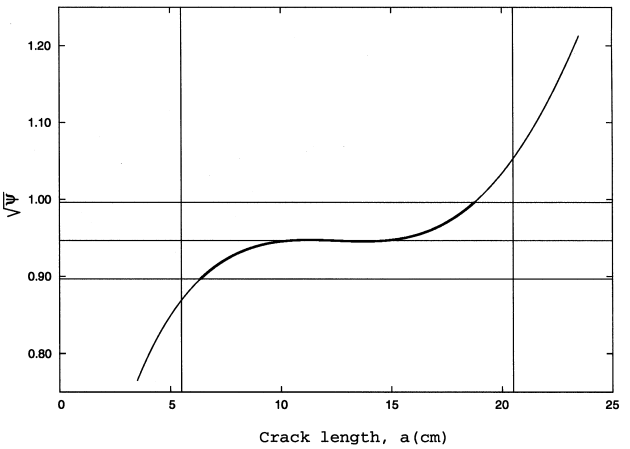

Fig. 6. The corrective function for K_I for the geometry called 'Specimen 2' ($L = 25\,\text{cm}$, $W = 10\,\text{cm}$, $d = 7\,\text{mm}$, $d_n/d = 1$, $g_w = 0\,\text{mm}$, $nl = 2\,\text{cm}$, $c = 4$). The vertical lines delimit the range explored in the present analysis. The horizontal lines define the operational range where K_I is constant within 5% (thick line).

Table 7
The power law parameters obtained by linear fit of the $v-K_I$ curves in Figs. 3 and 4. The geometrical parameters of Specimen 1 were $L = 17\,\text{cm}$, $W = 10\,\text{cm}$, $d = 7\,\text{mm}$, $d_n/d = 1/2$, $g_w = 2\,\text{mm}$, $nl = 2\,\text{cm}$, $c = 4$. Specimen 2 had $L = 25\,\text{cm}$, $W = 10\,\text{cm}$, $d = 7\,\text{mm}$, $d_n/d = 1$, $g_w = 0\,\text{mm}$, $nl = 2\,\text{cm}$, $c = 4$. The initial and final crack lengths for each test were reported and a symbol 'v' was marked in last column if the whole relaxation took place inside the range in which K_I is constant within 5%

Specimen 1	a_i (cm)	a_f (cm)	n	log A	Match
Real parameters			40.0	−3	
Operational range	5.4	10.1			
Explored range	4.5	12.5			
Estimated parameters	4.5	5.1	25.8	−4.5	x
	5.4	6.2	32.3	−3.8	v
	6.0	7.0	34.5	−3.6	v
	7.0	8.1	35.1	−3.3	v
	8.0	9.4	31.3	−3.1	v
	8.4	10.0	28.3	−3.0	v
	9.0	11.3	20.9	−2.8	x
	9.3	12.4	14.4	−2.8	x
Specimen 2					
Real parameters			40.0	−3	
Operational range	6.4	18.8			
Explored range	5.5	20.5			
Estimated parameters	5.5	5.6	33.2	−5.3	x
	6.0	6.2	33.8	−5.0	x
	6.4	6.6	34.3	−4.8	v
	7.0	7.3	35.1	−4.5	v
	8.0	8.5	36.5	−4.2	v
	9.0	9.6	37.9	−4.0	v
	10.0	10.7	39.0	−3.9	v
	11.0	11.7	39.9	−3.9	v
	12.0	12.7	40.3	−3.9	v
	13.0	13.8	40.1	−3.9	v
	14.0	14.8	39.1	−3.9	v
	15.0	15.9	37.1	−3.9	v
	16.0	17.1	33.8	−3.8	v
	17.1	18.6	28.5	−3.6	v
	18.1	20.4	21.2	−3.3	x

(c) increment of the crack length about $da = v\mathrm{d}t$ where $\mathrm{d}t$ is the time step of the simulation;
(d) calculate the new load corresponding to the new crack length using Eq. (10);
(e) repeat from (a) using the new values of load and crack length.

Each simulation was iterated for a total time of 100 s. The relaxation curves obtained were then analyzed with the classical Evans' method producing the $v-K_I$ curves reported in Figs. 7 and 8 together with the theoretical curve (thicker line). Substantial differences and a remarkable scatter are immediately apparent. Increasing the initial crack length, the location of the estimated curves moves progressively upwards in the bilogarithmic $v-K_I$ diagram. The shape of the curve gradually departs from linearity when the crack tip is near the borders of the explored range. In fact, in these regions the corrective coefficient ψ is rapidly changing in a non-linear way as the crack length increases during the test. The slope of those curves is reduced proportionally to the local slope of the corrective curve $\psi(a)$. The values of the stress-corrosion index of such curves were calculated by a least-squares linear fit and the results are reported in Table 7. To test the stability of the results, the simulations were performed with two different time steps (0.5 and 0.1 s), and consistent results were obtained.

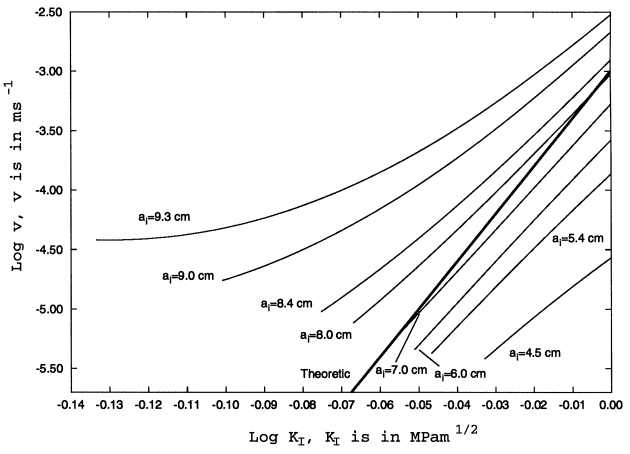

Fig. 7. The $v-K_I$ curves obtained by applying Evans' analysis to some relaxation experiments simulated with the aid of the corrective curves for the Specimen 1. The initial load is the same for all experiments, the different values of the initial crack length are indicated for each curve.

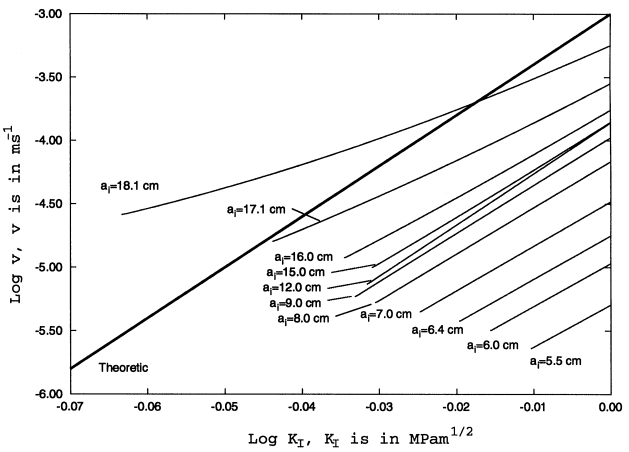

Fig. 8. The $v-K_I$ curves obtained by applying Evans' analysis to some relaxation experiments simulated with the aid of the corrective curves for the Specimen 2. The initial load is the same for all experiments, the different values of the initial crack length are indicated for each curve.

The simulations in which the initial and final crack lengths were both within the conservative operational range (in which K_I is constant within 5%) are indicated with a symbol 'v' in Table 7. The first important result is that Evans' analysis underestimates the stress-corrosion index up to 30% even operating in this range. As a consequence, this definition of the operational range is insufficient for accurate estimates of the stress-corrosion index with the classical Evans' approach.

An attempt to salvage the classical Evans' approach could still be made by defining a new operational range in which the underestimate on n itself is limited to 5%. Unfortunately, for Specimen 1, the smaller error obtained for n is about 12%, making the definition of such a range impossible. As for Specimen 2, the errors on n could be limited to 5% only if the whole relaxation were performed in a very narrow operational range of crack lengths (from 9 to 15 cm on a 25 cm long specimen, see Table 7). This constraint is a very strong one, since the attempts to produce an initial crack with a length in such a tight range would lead to discard most specimens. Moreover, the possibility of performing multiple relaxation tests on the same specimen would be considerably reduced.

On the contrary, by applying our corrective procedure there is no need to comply to such tight constraints, since the use of the corrective curves allows one to obtain accurate results working in a range that is much larger than the one required to obtain reliable estimates of n by using the classical Evans' method. The range left unexplored by our finite-element analysis is just five centimeters from each end of the specimen, which, for example, implies operational crack lengths covering a comfortable 15 cm range on 25 cm-long specimens. Table 7 shows that in this interval the classical Evans' analysis would produce underestimates up to 65%.

7. Conclusions

The exhaustive finite-element analysis performed by Ciccotti [2] showed that Evans' analytical

approximation gives an unsatisfactory description of the double-torsion loading configuration, except in a very narrow region of crack propagation in very thin specimens. The relative corrective coefficients were calculated.

A full methodology has been presented here to apply these corrective coefficients to calculate the characteristic $v-K_I$ curve of subcritical crack growth. The most important effect of the corrective coefficients is that not only the location of the curves is changed, but also their shape, generally increasing the slope. In other words, substantial modifications are induced on the stress-corrosion index, which is the most interesting parameter of subcritical crack-growth under a physical modeling point of view.

According to two numerical experiments of load relaxation at constant displacement that we performed, the neglection of the corrective coefficients leads to underestimating the stress-corrosion index up to 30% even if the relaxation takes place in the classical "optimal" operational range of crack lengths, where the variations of K_I do not exceed 5%. On the contrary, the use of the corrective coefficients allows one to obtain accurate estimates by using a wide range of specimen geometries and operational crack lengths. Furthermore, our corrective coefficients are based on a finite-element model which takes into account the influence of all the geometrical parameters of a real specimen, i.e., the presence of a side groove, its depth and width, the presence of an initial notch of given length, and the inclination of the curved crack front.

References

[1] Evans AG. A method for evaluating the time-dependent failure characteristics of brittle materials — and its applications to polycrystalline alumina. J Mater Sci 1972;7:1137–46.
[2] Ciccotti M. A realistic finite-element model for the double torsion loading configuration. J Am Ceram Soc 2000, in press.
[3] Atkinson BK. Technical note. Int J Rock Mech Min Sci Geomech Abstr 1979;16:49–53.
[4] Williams DP, Evans AG. A simple method for studying slow crack growth. J Test Eval 1973;1:264–270.
[5] Timoshenko S, Goodier JN. Theory of elasticity, 2nd ed. New York: McGraw Hill, 1951. p. 277.
[6] Pollet JC, Burns SJ. Crack velocity correction factor for the crack-front shape in double-torsion specimens. J Am Ceram Soc 1979;62:426–7.
[7] Atkinson BK. Subcritical crack growth in geological materials. J Geophys Res 1984;89:4077–114.
[8] Swanson PL. Subcritical crack growth and other time- and environment-dependent behavior in crustal rocks. J Geophys Res 1984;89(B6):4137–52.
[9] Fuller Jr ER. An evaluation of double-torsion testing — analysis. In: Fracture mechanics applied to brittle materials, Vol. ASTM STP 678. American Society of Testing Materials, 1979. p. 3–18.
[10] Pletka BJ, Fuller Jr ER, Koepke BG. An evaluation of double-torsion testing — experimental. In: Fracture mechanics applied to brittle materials, Vol. ASTM STP 678. American Society of Testing Materials, 1979. p. 19–37.
[11] Virkar AV. Gordon RS. Crack front profiles in double-torsion specimens. J Am Ceram Soc 1975;58:536–7.
[12] Pabst RF, Weick J. Double torsion measurements with and without a guiding notch. J Mater Sci 1981;16:836–8.
[13] Shetty DK, Virkar AV. Determination of the useful range of crack length in double torsion specimens. J Am Ceram Soc 1978;61:93–4.
[14] Trantina GG. Stress analysis of the double torsion specimen. J Am Ceram Soc 1977;60:338–41.